

# SER estimation method for 56 GBaud PAM-4 transmission system

Aadil Raza<sup>1</sup>, Kangping Zhong<sup>2,\*</sup>, Salman Ghafoor<sup>3,\*\*</sup>, Saeed Iqbal<sup>1</sup>,  
Muhammad Adeel<sup>2</sup>, Shahid Habib<sup>1</sup>, Muhammad Fasih Uddin Butt<sup>1</sup>, and Chao Lu<sup>2</sup>

<sup>1</sup>COMSATS Institute of Information Technology (CIIT), Islamabad, Pakistan

<sup>2</sup>Department of Electronic and Information Engineering, The Hong Kong Polytechnic University, Hong Kong, China

<sup>3</sup>National University of Sciences and Technology (NUST), Islamabad, Pakistan

\*Corresponding author: kangping.zhong@macom.com; \*\*corresponding author: salman.ghafoor@seecs.edu.pk

Received February 6, 2018; accepted February 9, 2018; posted online March 26, 2018

In this Letter, we have proposed a generalized Gaussian probability density function (GGPDF)-based method to estimate the symbol error ratio (SER) for pulse amplitude modulation (PAM-4) in an intensity modulation/direct detection (IM/DD) system. Furthermore, a closed form expression of  $SER_{GGD}$  for PAM-4 has been derived. The performance of the proposed method is evaluated through simulation as well as experimental work. The fitting of probability density functions of the received signal is applied via GGPDF and shape parameters  $P_1$  and  $P_2$  associated with different PAM-4 levels are determined. The optimum single value of shape parameter  $P$  is then calculated to estimate the SER. The mathematical relationship of  $P$  with different received optical powers and receiver bandwidths has been determined and verified. The proposed method is a fast and accurate method to estimate SER of a PAM-4 system, which is more reliable and in agreement with the error counting method.

OCIS codes: 060.4510, 060.2330.

doi: 10.3788/COL201816.040604.

The ever-growing bandwidth requirement of data centers and high speed optical interconnects has been driving researchers to design efficient, short reach optical transmission systems to realize 400 Gbit/s or even higher speeds. In the literature, many advanced modulation formats, such as pulse amplitude modulation (PAM-N), carrier-less amplitude and phase modulation (CAP), and discrete multi-tone (DMT), along with digital signal processing (DSP) have been employed in intensity modulation/direct detection (IM/DD) systems instead of a coherent system to achieve low cost short reach links over bandwidth limited optical devices<sup>[1-3]</sup>. Although, all modulation formats have shown good performance, but PAM-4 has been considered as a strong candidate by the IEEE P802.3bs 400 GbE task force due to the relaxed optical signal-to-noise-ratio (OSNR) requirement and low implementation complexity. The performance evaluation of a communication system is based upon the bit error ratio (BER) using the error counting method. However, this method requires a large number of symbols to calculate BER. Different analytical BER estimation methods have been proposed for non-return-to-zero (NRZ)-based quadrature phase shift keying (QPSK) systems with both linear and nonlinear impairments<sup>[4,5]</sup>. In Ref. [6], the symbol error ratio (SER) estimation method has been investigated for the multilevel PAM-N signaling format, which is based upon the  $Q$  factor metric. The  $Q$  factor depends upon statistical moments, such as mean and standard deviation of the received signal, which determine the probability density function (PDF). Furthermore, the authors in Ref. [6], presumed additive-white-Gaussian noise (AWGN), which provides an accurate  $SER_Q$  estimation for a low

$Q$  function and higher PAM-N format, such as PAM-8 and PAM-16. However, this accuracy deviates as the  $Q$  function goes higher and the PAM-N order decreases, such as PAM-4 and PAM-2. The reason for such deviation is the presence of noise at both the transmitter and receiver sides, which is not exactly Gaussian and provides inaccurate SER estimation. Therefore, it is required to determine the accurate distribution of non-AWGN associated with the received signal. A detailed statistical analysis of generalized Gaussian PDF (GGPDF) can be applied on the noise distribution to manipulate the shape parameters. In literature, different techniques have been demonstrated for determining the shape parameter of GGPDF<sup>[7-9]</sup>. In Ref. [10], a technique has been reported to find the value of the shape parameter by equating the  $SER_C$  from error counting with the calculated  $SER_{GGD}$  for polarization-multiplexed QPSK (PM-QPSK). These studies motivated us to investigate the PAM-4 system to provide an accurate estimation of SER based on shape parameter. To the best of the authors' knowledge, this has not been explored for a PAM-4-based system so far and needs to be investigated in depth.

In this Letter, we proposed a method based on GGPDF for accurately estimating SER for the PAM-4-based IM/DD system. The shape parameter dependent GGPDF fitting is applied to each level of the PAM-4 signal. The shape parameter  $P_1$  is used for both  $-3$  and  $-1$  levels, and shape parameter  $P_2$  is used for both  $+1$  and  $+3$  levels. Based on  $P_1$  and  $P_2$  values, a single value of shape parameter  $P$  is determined to estimate SER. Our method provides a faster way to accurately estimate SER for PAM-4.

The generalized expression for GGPDF is given in Eq. (1)<sup>[1]</sup>:

$$f(x;\mu,\sigma,P) = \frac{1}{2\Gamma(1+1/P)A(P,\sigma)} \exp\left\{-\left[\frac{|x-\mu|}{A(P,\sigma)}\right]^P\right\}, \quad (1)$$

where  $A(P,\sigma) = \left[\frac{\sigma^2\Gamma(1/P)}{\Gamma(3/P)}\right]^{1/2}$ , and  $\mu$ ,  $\sigma$ ,  $P$ , and  $\Gamma$  are the mean, standard deviation, shape parameter, and gamma function, respectively. The Gaussian PDF is the special case of Eq. (1) for  $P = 2$ . The value of  $P$  determines the shape of GGPDF, which ultimately affects the tail probabilities. The proposed method for calculating  $\text{SER}_{\text{GGD}}$  uses  $\mu$ ,  $\sigma$ , and  $P$  associated with GGPDFs for all four levels of the PAM-4 signal. The generalized analytical expression for  $\text{SER}_{\text{GGD}}$  is given in Eq. (2)<sup>[2]</sup>:

$$\text{SER}_{\text{GGD}} = \frac{1}{\log_{10}(N)} \sum_{n=1}^N P(I_n)[P(I_{n-1}|I_n) + P(I_{n+1}|I_n)], \quad (2)$$

where  $N$  represents the order of the PAM signal, and  $n$  represents a specific level.  $P(I_n)$  is the probability of the signal being transmitted, whereas  $P(I_{n-1}|I_n)$  and  $P(I_{n+1}|I_n)$  are the conditional probabilities. The optimum threshold levels ( $\text{th}_1$ ,  $\text{th}_2$ , and  $\text{th}_3$ ) for PAM-4 are defined as follows:

$$\text{th}_1 = P_{\text{avg}} - \left(\frac{\text{OMA}_{\text{outer}}}{3}\right), \quad \text{th}_2 = P_{\text{avg}} \quad \text{and} \\ \text{th}_3 = P_{\text{avg}} + \left(\frac{\text{OMA}_{\text{outer}}}{3}\right),$$

where  $P_{\text{avg}}$  is the average power of the received histograms of all four levels, and optical modulation amplitude ( $\text{OMA}_{\text{outer}}$ ) is the difference between the outermost two levels. According to Eq. (2), an erroneous decision is made on both sides of the middle two levels, whereas for the outer two levels, it is made only on one side. With the assumption that all four levels of the PAM-4 signal are equiprobable, i.e.,  $P(I_1) = P(I_2) = P(I_3) = P(I_4) = 1/4$ , and the detailed expression for  $\text{SER}_{\text{GGD}}$  is derived and written in Eq. (3):

$$\text{SER}_{\text{GGD}} = \frac{1}{4} \left[ \int_{-\infty}^{\text{th}_1} f_{-1}(x;\mu,\sigma,P_1) dx + \int_{\text{th}_1}^{\infty} f_{-3}(x;\mu,\sigma,P_1) dx + \int_{-\infty}^{\text{th}_2} f_{+1}(x;\mu,\sigma,P_2) dx + \int_{\text{th}_2}^{\infty} f_{-1}(x;\mu,\sigma,P_1) dx + \int_{-\infty}^{\text{th}_3} f_{+3}(x;\mu,\sigma,P_2) dx + \int_{\text{th}_3}^{\infty} f_{+1}(x;\mu,\sigma,P_2) dx \right], \quad (3)$$

where  $f_{-3}$ ,  $f_{-1}$ ,  $f_{+1}$ , and  $f_{+3}$  are the PDFs of the PAM-4 levels. The shape parameter  $P_1$  is associated with  $f_{-3}$  and  $f_{-1}$ , whereas  $P_2$  is associated with  $f_{+1}$  and  $f_{+3}$ . The values of both  $P_1$  and  $P_2$  are now calculated by equating the  $\text{SER}_{\text{GGD}}$  with  $\text{SER}_C$ , obtained from the error counting method, and are used to find an optimum single value of  $P$ . This value of  $P$  is finally used to estimate SER.

The simulation setup is shown in Fig. 1. The pseudo-random bit sequence (PRBS) of length  $2^{16} - 1$  is used to generate the PAM-4 data signal. A single drive Mach-Zehnder modulator (MZM) is used to modulate the continuous wave (CW) laser source with a central wavelength of 1310 nm with PAM-4 data. The modulated data is transmitted over a standard single mode fiber (SSMF) of a length of 10 km. A variable optical attenuator (VOA) is used before the receiver to adjust received optical powers (ROPs). The transmitted optical signal is then detected by a photo diode (PD). The signal at the output of PD passes through a tunable fourth-order Bessel low-pass filter (LPF) which can operate at different bandwidths. It is used to analyze the bandwidth limitations of the transmission system. Finally, the received data is sent to offline DSP. The received signal was first normalized and then resampled to two samples per symbol to perform the retiming operation. A 5 tap T/2 adaptive equalizer via the least mean square (LMS) algorithm is used for the channel equalization. Finally, the symbol error by the counting method was calculated after the hard decision. Table 1 shows the simulation parameters used in our system. A detailed simulation study is carried out to evaluate the accuracy of our SER estimation method in different scenarios, especially for different receiver bandwidths. For this purpose, the contour plots are drawn, as shown in Fig. 2, for the receiver bandwidth of 30 GHz using Eq. (3). The range of values of  $P_1$  and  $P_2$  between 0 and 2.5 with an increment of 0.25 is used to obtain the optimum contour line, where matching (i.e.  $Z = \text{SER}_C - \text{SER}_{\text{GGD}} = 0$ ) between  $\text{SER}_C$  and  $\text{SER}_{\text{GGD}}$  is achieved. The desired contour line providing  $Z = 0$  can be seen from Figs. 2(a)-2(e) for ROPs of -4.41, -5.06, -5.71, -6.36, and -7.01 dBm. However,  $Z$  is not converging to zero, as shown in Fig. 2(f), for

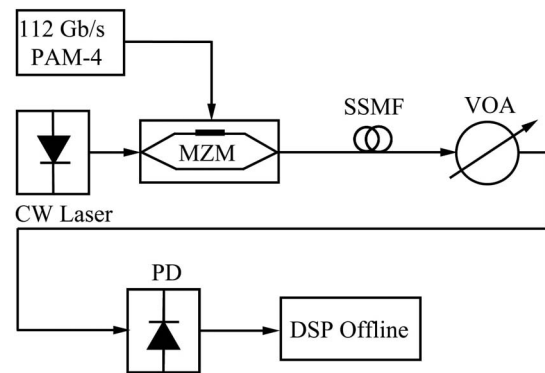


Fig. 1. Simulation setup of 56 GBaud PAM-4 transmission system.

**Table 1.** Simulation Parameters

Parameter	Values
Length (km)	10
Wavelength (nm)	1310
Linewidth (MHz)	5
Rx. BW (GHz)	18,19,20,25, and 30
Power (dBm)	0
PD thermal noise (pA/Hz <sup>0.5</sup> )	20
PD dark current (nA)	10
PD responsivity (A/W)	1

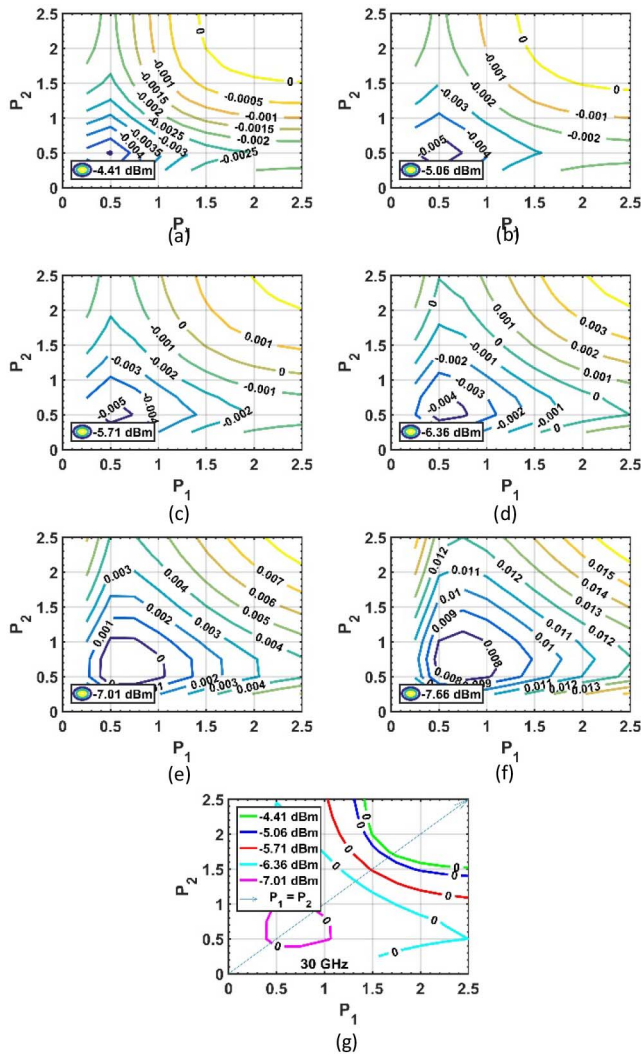


Fig. 2. Contour plots at (a)  $-4.41$  dBm, (b)  $-5.06$  dBm, (c)  $-5.71$  dBm, (d)  $-6.36$  dBm, (e)  $-7.01$  dBm, and (f)  $-7.66$  dBm for 30 GHz. (g) Contour lines at  $Z = 0$  for different ROPs at 30 GHz.

$-7.66$  dBm, and same is true for even lower ROPs. The reason for this can be understood by observing the SER, which tends to go higher with decreasing ROPs. The

PDF of the received signal at a higher SER loses its shape and does not provide  $n$  adequate  $P$  values, which ultimately cannot give a  $\text{SER}_{\text{GGD}}$  equal to  $\text{SER}_C$  at lower ROPs. The contour lines at  $Z = 0$  are combined in one figure for corresponding ROPs at 30 GHz, as shown in Fig. 2(g). The dashed arrow line is drawn diagonally, which is intersecting the contour lines and provides a single optimum value of  $P$ .

Similarly, the system is also analyzed for four more receivers' bandwidths, which are 18, 19, 20, and 25 GHz. The obtained contour lines at  $Z = 0$  for corresponding ROPs at the mentioned receivers' bandwidths are shown in Figs. 3(a)–3(d), respectively.

The SER as a function of ROPs for all receiver bandwidths is shown in Fig. 4(a). The receiver sensitivities for the forward error correction (FEC) limit at a SER of  $7.6 \times 10^{-3}$  are  $-5.80$ ,  $-6.75$ ,  $-7.20$ ,  $-7.66$ , and  $-7.66$  dBm for 18, 19, 20, 25, and 30 GHz, respectively. It may be noted that SER improves when the receiver bandwidth increases and shows no improvement after 30 GHz<sup>[12]</sup>. Figure 4(b) shows the contour lines at a fixed ROP of  $-5.71$  dBm for all receiver bandwidths to observe the  $P$  value dependence over different bandwidths. Figure 4(c) shows the  $P$  as a function of ROPs at different receiver bandwidths. It may be observed that the  $P$  value increases nonlinearly with the increase in ROPs for all bandwidths. It may be seen that at higher ROPs, the variation in the  $P$  value is smaller as compared to lower ROPs with respect to the bandwidths. This implies that the shape of the PDF is degraded at lower ROPs. The dependence of  $P$  on the receiver bandwidth is plotted in Fig. 4(d). It may be observed that the value of  $P$  increases with the increase in bandwidth and becomes constant at higher bandwidths.

Due to the dependence of shape parameter  $P$  on receiver bandwidth ( $B$ ) and ROP ( $P_{\text{ROP}}$ ), we have determined a third-order two-variable-based function  $f(B, P_{\text{ROP}})$  for finding the optimum  $P$  value. For this purpose, we have

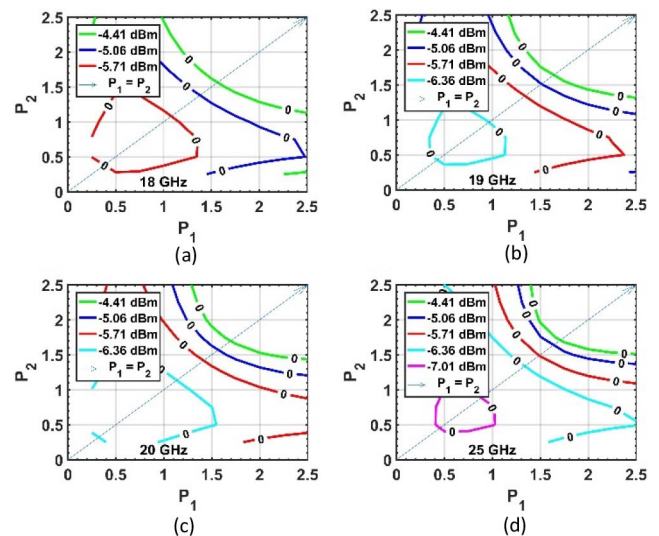


Fig. 3. Contour lines at  $Z = 0$  for different ROPs at (a) 18 GHz, (b) 19 GHz, (c) 20 GHz, and (d) 25 GHz.

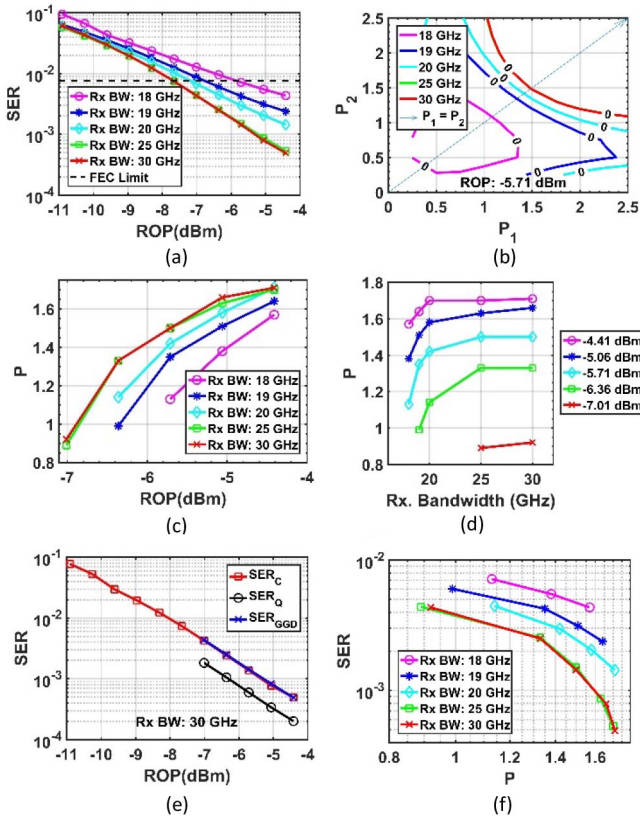


Fig. 4. (a) SER versus ROPs at different bandwidths. (b) Contour plot at  $-5.71$  dBm for 18, 19, 20, 25, and 30 GHz. (c)  $P$  versus ROPs for 18, 19, 20, 25, and 30 GHz. (d)  $P$  versus receiver bandwidths at  $-4.41$ ,  $-5.06$ ,  $-5.71$ ,  $-6.36$ , and  $-7.01$  dBm. (e) Comparison among  $SER_C$ ,  $SER_Q$ , and  $SER_{GGD}$  as a function of ROPs at 30 GHz. (f) SER versus  $P$  for 18, 19, 20, 25, and 30 GHz at 10 km.

used the curve fitting (or function estimation) technique to find a mathematical relationship from the curve data points of Figs. 4(c) and 4(d)<sup>[13]</sup>. There are different fitting methods available to be used for the evaluation for specific cases. We have used the polynomial fit method to map our curve data points to a polynomial function. The resultant calibration equation is given by

$$P = f(B, P_{ROP}) = a_0 + a_1 B + a_2 P_{ROP} + a_3 B^2 + a_4 B P_{ROP} + a_5 P_{ROP}^2 + a_6 B^3 + a_7 B^2 P_{ROP} + a_8 B P_{ROP}^2 + a_9 P_{ROP}^3, \quad (4)$$

where  $a_0 = -2.322$ ,  $a_1 = 1.485$ ,  $a_2 = 4.622$ ,  $a_3 = -0.071$ ,  $a_4 = -0.102$ ,  $a_5 = 0.657$ ,  $a_6 = 0.001$ ,  $a_7 = 0.002$ ,  $a_8 = 0.002$ , and  $a_9 = 0.049$ . The polynomial fit method calculates the different statistical parameters, like the sum of squares due to error (SSE) 0.00879, R-square 0.9945, adjusted R-square 0.9912, and root mean squared error (RMSE) 0.02421. The values of these parameters determine how accurately the obtained model fits to the curve data points. The values obtained for different parameters in our case are very good, and the obtained relationship gives a very good approximation of

$SER_{GGD}$  (blue line), which agrees with  $SER_C$ , as shown in Fig. 4(e). The  $SER_Q$  using Gaussian approximation, when  $P = 2$ , is plotted in Fig. 4(e), and it can be clearly seen that, as expected, it underestimates the  $SER_C$ . The dependence of SER on  $P$  for different receiver bandwidths is plotted in Fig. 4(f). The calibration equation can be implemented in a straightforward way on a suitable hardware platform, such as a field programmable gate array (FPGA) using VHDL/Verilog or DSP using C/assembly language. Figures 5(a) and 5(b) show the eye diagram, where  $SER = 7.6 \times 10^{-3}$  is attained, as shown in Fig. 4(a), and the PDF of the received symbol of PAM-4 at  $-7.66$  dBm for 30 GHz, respectively.

The experimental setup designed for a 56 Gbaud PAM-4 transmission system is presented in Fig. 6. A  $2^{16}$  de Bruijn bit sequence is used for bit to symbol mapping, and a PAM-4 signal is generated. The PAM-4 signal is then loaded into an arbitrary waveform generator (AWG) for the generation of an electrical signal. The electrical signal is amplified using a linear electrical amplifier (EA) and modulated with an externally modulated laser (EML) having a 3 dB bandwidth of 20 GHz. The biasing voltage of the EML is adjusted and optimized. The modulated signal is transmitted over a 10 km SSMF towards the receiver side. A VOA is deployed before the receiver for the adjustment of ROP. The receiver is composed of a positive-intrinsic-negative (PIN) diode and a transimpedance amplifier having a 3 dB bandwidth of 30 GHz. The signal detected at the receiver is captured by an 80 GS/s digital sampling oscilloscope (DSO).

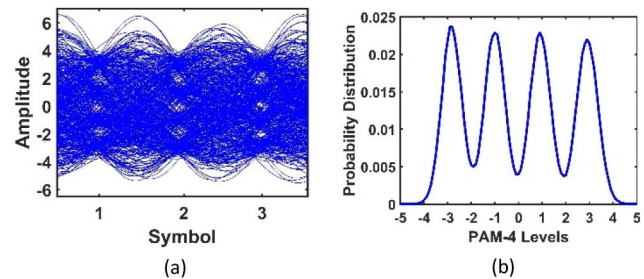


Fig. 5. (a) Eye-diagram and (b) probability distribution function of the received signal of PAM-4 at  $-7.66$  dBm at 30 GHz.

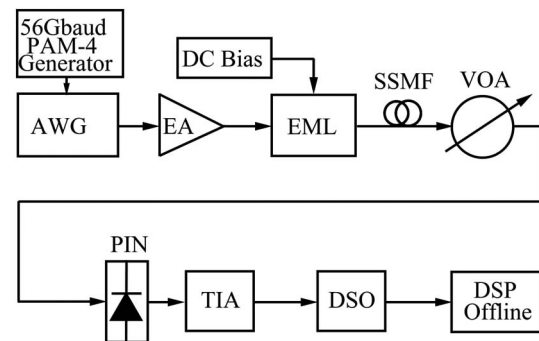


Fig. 6. Experimental setup of 56 Gbaud PAM-4 transmission system.

Finally, the offline DSP is used in the same manner as that used for the simulation setup to obtain the desired results. The detailed results obtained from the experimental study are shown in Figs. 7 and 8. The system performance is analyzed for the two cases: back-to-back (BtB) and 10 km. The obtained contour lines at  $Z = 0$  for corresponding ROPs are combined and are shown in Figs. 7(a) and 7(b) for BtB and 10 km, respectively. The SER as a function of ROPs for both BtB and 10 km is shown in Fig. 7(c). The performance of 10 km transmission is better than BtB. The reason for this better performance is the suppression of chirp induced by EML with the dispersion factor of a 10 km SSMF<sup>[14]</sup>. The optimum value of  $P$  is then calculated in a similar manner to that used for the simulation data. The dependence of  $P$  on

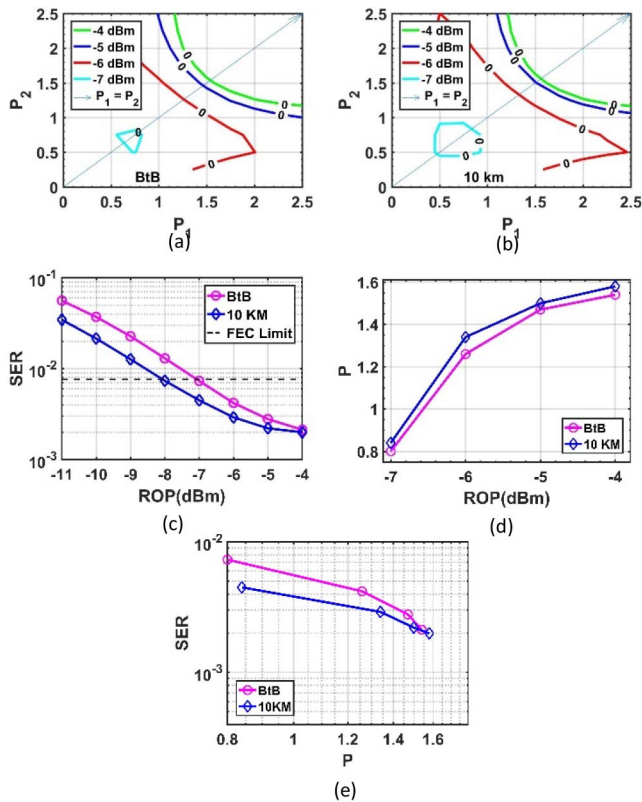


Fig. 7. Contour lines at  $Z = 0$  for  $-4, -5, -6, -7$ . (a) BtB. (b) 10 km. (c) SER versus ROPs for BtB and 10 km. (d)  $P$  versus ROPs at BtB and 10 km. (e) SER versus  $P$  at BtB and 10 km.

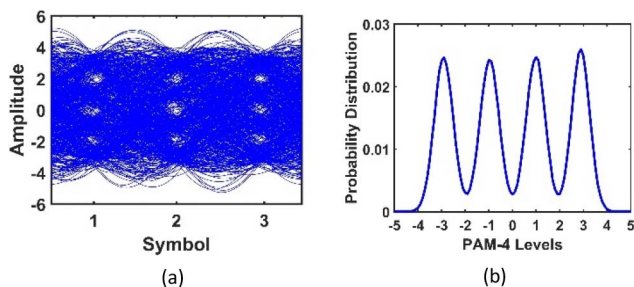


Fig. 8. (a) Eye-diagram and (b) probability distribution function of the received signal of PAM-4 at  $-7$  dBm at 10 km.

ROPs and the dependence of SER on  $P$  are plotted in Figs. 7(d) and 7(e) for both BtB and 10 km. It may be observed that  $P$  becomes higher with increasing ROPs, and SER decreases with increasing  $P$ . Figures 8(a) and 8(b) show the eye diagrams, where SER  $7.6 \times 10^{-3}$  is attained, as shown in Fig. 7(c), and the PDF of the received symbol of PAM-4 levels at  $-8$  dBm for 10 km. In a nutshell, the results obtained from both the simulation and experiment are verified for a variety of cases, like different ROPs, receiver's bandwidths, and fiber lengths. Due to limited bandwidths of components, the experimental result is only achieved for a specific case of EML having a 3 dB bandwidth of 20 GHz and a PIN diode and transimpedance amplifier having a 3 dB bandwidth of 30 GHz. Based on these results, it may be deduced that  $P$  has a relationship with ROPs, receiver bandwidths, and fiber length. These results show that for a variety of scenarios our proposed method provides an accurate and faster SER estimation as compared to the error counting method for PAM-4-based IM/DD optical transmission systems.

In conclusion, a method based on GPDF has been demonstrated by simulation and experiment for estimating SER of PAM-4 in the IM/DD system. A closed form expression of  $SER_{GGD}$  for PAM-4 has been derived. The GPDF is used to determine shape parameter  $P$  to calculate the SER. A mathematical relationship of  $P$  with the receiver bandwidth and ROPs has been determined and verified. It is concluded that SER estimation using GPDF provides a faster way to get accurate agreement with  $SER_C$ .

## References

1. K. P. Zhong, W. Chen, Q. Sui, M. J. Wei, A. P. T. Lau, C. Lu, and L. Zeng, in *Proceedings of OFC* (2015), paper TH3A.3.
2. K. P. Zhong, X. Zhou, Y. Gao, W. Chen, J. Man, L. Zeng, A. P. T. Lau, and C. Lu, *Photon. Technol. Lett.* **27**, 1757 (2015).
3. N. Eiselt, J. Wei, H. Griesser, A. Dochhan, M. Eiselt, J. Elbers, J. J. V. Olmos, and I. T. Monroy, in *Proceedings of OFC* (2016), paper W1K.5.
4. G. Goldfarb and G. Li, *Opt. Express* **14**, 8043 (2006).
5. F. Zhang, Y. Gao, Y. Luo, Z. Chen, and A. Xu, *Opt. Express* **18**, 9 (2010).
6. M. Chagnon, M. Osman, M. Poulin, C. Latrasse, J. Gagne, Y. Painchaud, C. Paquet, S. Lessard, and D. Plant, *Opt. Express* **22**, 21018 (2014).
7. S. B. Weinstein, *IEEE Trans. Commun. Technol.* **19**, 6 (1971).
8. M. K. Varanasi and B. Aazhang, *J. Acoust. Soc. Am.* **86**, 1404 (1989).
9. N. Stojanovic, *IEEE Trans. Signal Process.* **57**, 270 (2009).
10. J. C. Cartledge, J. D. Downie, J. E. Hurley, X. Zhu, and I. Roudas, *J. Lightwave Technol.* **30**, 10 (2012).
11. M. C. Jeruchim, *IEEE J. Sel. Areas Commun.* **SAC-2**, 1 (1984).
12. M. A. Mestre, H. Mardoyan, C. Caillaud, R. Rios-Muller, J. Renaudier, P. Jenneve, F. Blache, F. Pommereau, J. Decober, F. Jorge, P. Charbonnier, A. Konczykowska, J.-Y. Dupuy, K. Mekhazni, J.-F. Paret, M. Faugeron, F. Mallecot, M. Achouche, and S. Bigo, *J. Lightwave Technol.* **34**, 7 (2016).
13. J. H. Mathews and K. K. Fink, *Numerical Methods Using Matlab* (Pearson, 2004).
14. K. P. Zhong, X. Zhou, Y. Gao, W. Chen, J. Man, L. Zeng, A. P. T. Lau, and C. Lu, *IEEE Photon. Technol. Lett.* **27**, 1757 (2015).